Development of Correlations for Windage Power Losses Modeling in an Axial Flux Permanent Magnet Synchronous Machine with Geometrical Features of the Magnets

Authors:

Alireza Rasekh, Peter Sergeant, Jan Vierendeels

Date Submitted: 2019-02-27

Keywords: Computational Fluid Dynamics, magnet parameters, windage losses, AFPMSM

Abstract:

In this paper, a set of correlations for the windage power losses in a 4 kW axial flux permanent magnet synchronous machine (AFPMSM) is presented. In order to have an efficient machine, it is necessary to optimize the total electromagnetic and mechanical losses. Therefore, fast equations are needed to estimate the windage power losses of the machine. The geometry consists of an open rotor?stator with sixteen magnets at the periphery of the rotor with an annular opening in the entire disk. Air can flow in a channel being formed between the magnets and in a small gap region between the magnets and the stator surface. To construct the correlations, computational fluid dynamics (CFD) simulations through the frozen rotor (FR) method are performed at the practical ranges of the geometrical parameters, namely the gap size distance, the rotational speed of the rotor, the magnet thickness and the magnet angle. Thereafter, two categories of formulations are defined to make the windage losses dimensionless based on whether the losses are mainly due to the viscous forces or the pressure forces. At the end, the correlations can be achieved via curve fittings from the numerical data. The results reveal that the pressure forces are responsible for the windage losses for the side surfaces in the air-channel, whereas for the surfaces facing the stator surface in the gap, the viscous forces mainly contribute to the windage losses. Additionally, the results of the parametric study demonstrate that the overall windage losses in the machine escalate with an increase in either the rotational Reynolds number or the magnet thickness ratio. By contrast, the windage losses decrease once the magnet angle ratio enlarges. Moreover, it can be concluded that the proposed correlations are very useful tools in the design and optimizations of this type of electrical machine.

Record Type: Published Article

Submitted To: LAPSE (Living Archive for Process Systems Engineering)

Citation (overall record, always the latest version):	LAPSE:2019.0320
Citation (this specific file, latest version):	LAPSE:2019.0320-1
Citation (this specific file, this version):	LAPSE:2019.0320-1v1

DOI of Published Version: https://doi.org/10.3390/en9121009

energies

MDPI

Article

Development of Correlations for Windage Power Losses Modeling in an Axial Flux Permanent Magnet Synchronous Machine with Geometrical Features of the Magnets

Alireza Rasekh [1,*], Peter Sergeant [2,3] and Jan Vierendeels [1]

1 Department of Flow, Heat and Combustion Mechanics, Faculty of Engineering and Architecture, Ghent University, B-9000 Ghent, Belgium; Jan.Vierendeels@UGent.be
2 Department of Electrical Energy, Systems and Automation, Faculty of Engineering and Architecture, Ghent University, B-9000 Ghent, Belgium; Peter.Sergeant@UGent.be
3 Flanders Make, the Strategic Research Centre for the Manufacturing Industry, B-8500 Kortrijk, Belgium
* Correspondence: Alireza.Rasekh@UGent.be; Tel.: +32-9-2649521

Academic Editor: David Wood
Received: 13 October 2016; Accepted: 25 November 2016; Published: 30 November 2016

Abstract: In this paper, a set of correlations for the windage power losses in a 4 kW axial flux permanent magnet synchronous machine (AFPMSM) is presented. In order to have an efficient machine, it is necessary to optimize the total electromagnetic and mechanical losses. Therefore, fast equations are needed to estimate the windage power losses of the machine. The geometry consists of an open rotor–stator with sixteen magnets at the periphery of the rotor with an annular opening in the entire disk. Air can flow in a channel being formed between the magnets and in a small gap region between the magnets and the stator surface. To construct the correlations, computational fluid dynamics (CFD) simulations through the frozen rotor (FR) method are performed at the practical ranges of the geometrical parameters, namely the gap size distance, the rotational speed of the rotor, the magnet thickness and the magnet angle. Thereafter, two categories of formulations are defined to make the windage losses dimensionless based on whether the losses are mainly due to the viscous forces or the pressure forces. At the end, the correlations can be achieved via curve fittings from the numerical data. The results reveal that the pressure forces are responsible for the windage losses for the side surfaces in the air-channel, whereas for the surfaces facing the stator surface in the gap, the viscous forces mainly contribute to the windage losses. Additionally, the results of the parametric study demonstrate that the overall windage losses in the machine escalate with an increase in either the rotational Reynolds number or the magnet thickness ratio. By contrast, the windage losses decrease once the magnet angle ratio enlarges. Moreover, it can be concluded that the proposed correlations are very useful tools in the design and optimizations of this type of electrical machine.

Keywords: AFPMSM; CFD; magnet parameters; windage losses

1. Introduction

Axial flux permanent magnet synchronous machines (AFPMSMs) are quite modern devices with extensive flexibility not only at high-speed-low-torque but also at low-speed-high-torque applications [1–3]. The former is typical for wind turbine applications as the major source of clean and sustainable energy supply. In this regard, any improvement in the performance of the AFPMSMs can make a great impact on the wind turbine industry. For further development of such a machine, the fundamental understanding of contributors to losses is absolutely essential. In AFPMSMs, the main

sources of losses include the copper losses, the iron losses and the mechanical losses [4]. The latter is composed of the bearing losses and windage losses. The proportion of windage losses is usually moderate, albeit not completely insignificant [5]. The electromagnetic analysis of an AFPMSM has been widely addressed [6–10]. For instance, several analytical models were developed to compute the iron losses accurately and in a fast way by Hemeida and Sergeant [11]. In contrast to the electromagnetic analysis, the issue of windage losses in this type of electrical machine is still debatable.

Windage power losses account for the power associated with the aerodynamic forces (viscous or pressure) against rotary parts of the machine. Vranick [12] pioneered the problem of the windage losses in rotating electrical machines. He developed a mathematical equation for drag losses in alternators. Wild et al. [13] presented a computational method of the flow in the axial gap of the rotor and the stator along with an experimental windage torque measurement. They indicated that Taylor vortices result in axial variations of the azimuthal shear stress. Anderson et al. [14] simulated air cooling and windage losses in a high-speed electric motor. They proposed correlations to ascertain the viscous force acting on the rotor of the motor that matched with the empirical data.

Most, if not all, literature in this field has considered the rotor as a simple rotating disk in an enclosure and thus the presence of the magnets at the rotor disk was neglected [15,16]. Within this framework, Coren et al. [17] presented experimental data for the windage losses associated with a rotating disk in a rotor–stator cavity with a superimposed throughflow of air at high rotational Reynolds numbers up to the range of $Re = 10^7$.

Nevertheless, the influence of the protrusion on the rotor on the moment coefficient for a rotor–stator system was investigated by Luo et al. [18]. They demonstrated that the gap size ratio has a limited impact on the friction torque. Liu et al. [19] shed light further on the effect of the protrusion parameter of the rotor disk on the windage losses in the rotor–stator system.

In general, the windage power losses in an AFPMSM, which is the focus of this research, have not been elaborately investigated in the precedent studies yet. Among few examples, Giovanni [20] carried out a computational fluid dynamics (CFD)-parametric study to calculate the windage losses in an AFPMSM concerning variable magnet thickness. He showed that an increase in the magnet groove depth from 2 to 18 mm can noticeably raise the windage losses (up to 60 W) through the generator with the rotor diameter of 220 mm, gap size distance of 2 mm and the angular velocity of 1500 rpm. Wrobel et al. [21] also performed CFD simulations to assess the windage losses in an AFPMSM. They investigated the aerodynamic effects occurring within the air-gap. It was found that the windage/drag loss generated in the analysed machine assembly is relatively minor compared to the bearing loss.

In order to have a complete electromagnetic and mechanical design of the machine, it is vital to have fast formulations to calculate all of the loss components in the machine. It is noteworthy to emphasize that building up the experimental set-up to measure the windage losses for all of the surface components of the machine is a very difficult task. The feasible alternative approach can be the numerical modeling, which is the purpose of this research work. Thus, the objective is to construct a set of correlations for predicting the windage loss occurring in an AFPMSM, based on numerical modeling. To achieve this, CFD simulations are performed for the practical ranges of geometrical parameters including the magnet thickness, the magnet angle, the air-gap distance as well as the rotational speed of the rotor. It should be mentioned that this numerical set-up has already been employed and succeeded in the convective heat transfer modeling of the AFPMSM [22]. Details of the proposed method and the results are discussed in the following sections.

2. Problem Set-Up and Numerical Modeling

Figure 1 illustrates the geometrical details of the rotor–stator system in the AFPMSM along with a schematic diagram of the rotor disk itself. The rated power of the machine is 4 kW. To facilitate the geometry parametrization procedure, the model is slightly simplified. For example, the shape of the real magnet is an isosceles trapezoid, while it is presumed here that the inner and the outer edges of the cross section of the magnets are part of the circles instead of the straight lines. The configuration

consists of two rotors and one stator in between, and only half of the geometry with a symmetry plane in the middle is studied. The right disk corresponds to the stator, and the left one is the rotor. The radius of the rotor and the stator are kept constant at 74 and 84 mm, respectively. There are sixteen magnets that are evenly distributed on the rotor side, facing the stator disk in the gap. In fact, this machine has eight pole pairs and the number of stator slots is 15. Thus, the pole pitch angle, which is the angular distance between two adjacent poles on the machine, is equal to $1/16 \times 360^\circ = 22.5^\circ$. Due to the cyclic flow, only $1/16$ of the whole system is taken into account. Furthermore, there is an annular opening at the rotor disk, allowing the airflow entering into the gap region for cooling purposes. The effects on the flow field of radial spokes, connecting the center of the rotor to the outer side across the annular opening, have been neglected.

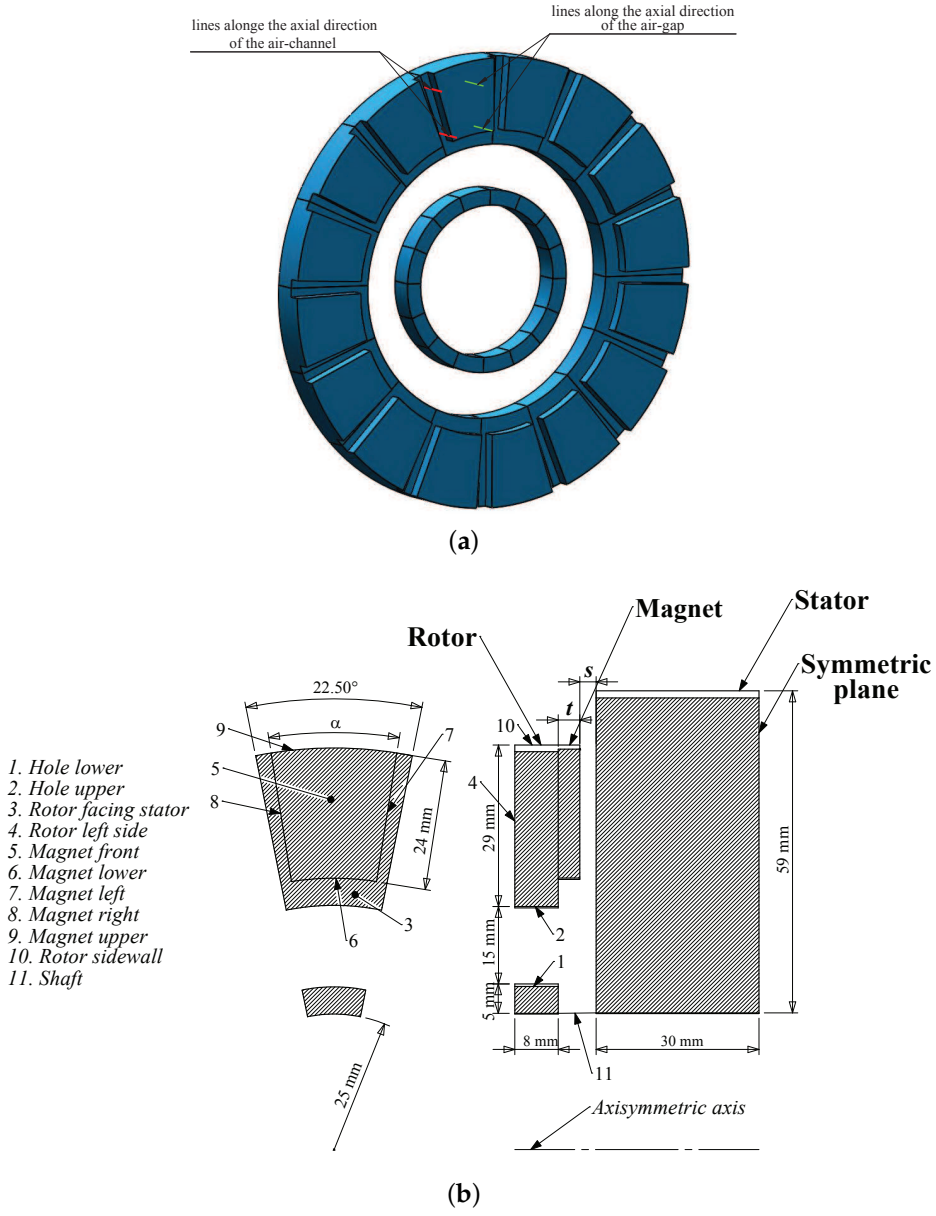

Figure 1. (**a**) The schematic diagram of the rotor in an AFPMSM; and (**b**) geometrical details of the current rotor-stator system.

The flow pattern in this configuration is governed by four non-dimensional numbers comprising the gap size ratio, $G = s/R$, the rotational Reynolds number, $Re = \omega R^2/\nu$, the magnet angle ratio,

$\alpha_m = \alpha \times 16/360$, and the magnet thickness ratio, $L = t/R$, where s is the air-gap thickness, R denotes the outer radius of the rotor, ω is the angular velocity of the rotor, ν represents the kinematic viscosity of air, α is the magnet angle, and t denotes the magnet thickness as shown in Figure 1b. The practical ranges of these parameters are $0.0068 \leq G \leq 0.0811$, $3.5 \times 10^4 \leq Re \leq 3.5 \times 10^5$, $0.7 \leq \alpha_m \leq 0.9$ and $0.0270 \leq L \leq 0.0811$. These ranges account for the magnet tip velocity of 10–100 m/s (equivalent to the angular velocity of 1290.4–12,904 rpm), the gap thickness of 0.5–6 mm, the magnet angle of 15.75°–20.25° and the magnet thickness of 2–6 mm.

It is assumed that the surfaces are isothermal, since the thermal conductivities of the materials in the rotor and the stator are rather high. The variation of the air density with temperature is considered by modeling air as an incompressible ideal gas. In addition, the air viscosity varies with temperature according to Sutherland's viscosity law. The Reynolds number is evaluated at the temperature of $\frac{T_r + T_s + T_{amb}}{3}$, where T_r represents surface temperature of the rotor, T_s denotes the surface temperature of the stator and T_{amb} is ambient temperature.

The frozen rotor (FR) model that yields the steady state solution is employed for the numerical modeling. This approach is used in cases where the rotor–stator interaction is not strong. In fact, for the machine under consideration, the flow is steady since the stator surface is smooth and also the influence of the natural convection is negligible. Consequently, the results of the FR method will be the same as when sliding interfaces would have been used. In the FR method, the computational mesh remains fixed and the flow field is solved using the equations adapted for the moving reference frame. As shown in Figure 2, the computational domain is divided into the rotary and the stationary parts by an interface which is situated in the middle of the gap between the magnet and the stator. The governing equations in each subdomain are written with respect to the subdomain's reference frame; nevertheless, the velocities in each subdomain are calculated in the absolute frame. Thus, no further transformation is required at the interface between the rotary and the stationary subdomain. The atmospheric pressure boundary is placed far away from the rotor.

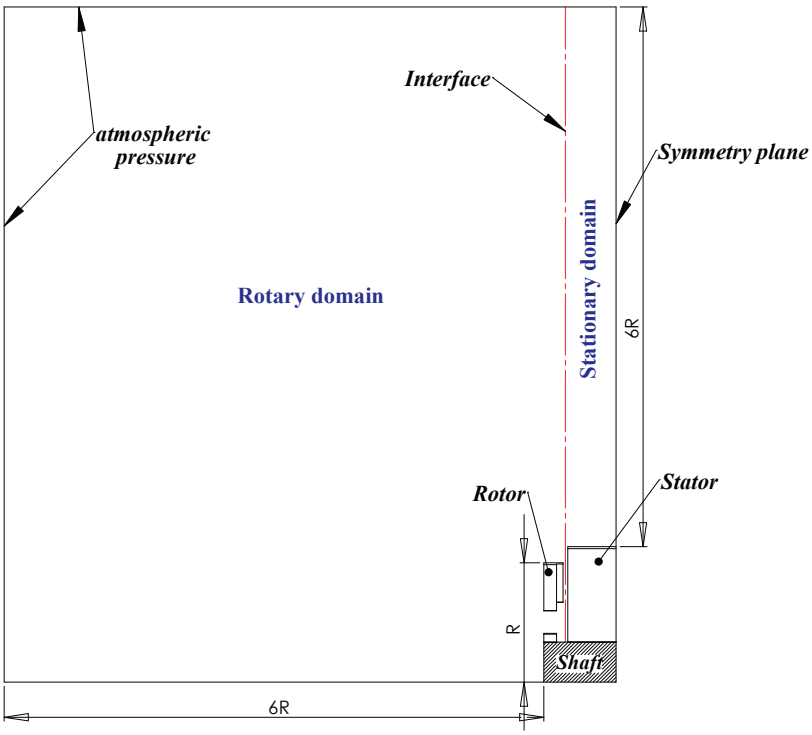

Figure 2. Side view of the computational domain.

3. Numerical Results

In order to have adequate data for constructing the model for the windage losses, CFD simulations are performed. To do so, the commercial CFD software Ansys FLUENT (14.5.7) has been utilized to simulate the 3D flow fields. For the case of the air-gap thickness of 1.0 mm, the tip velocity of a magnet of 30 m/s, the magnet angle of 18°, the magnet thickness of 4.0 mm along with the surface temperatures of $T_s = 120$ °C and $T_r = 100$ °C are chosen as reference points for this parametric study. This represents the non-dimensional numbers of $G = 0.0135$, $Re = 1.06 \times 10^5$, $\alpha_m = 0.8$ and $L = 0.0540$. The 3D computational domain is composed of 2,944,000 nodes of hexahedral mesh type. To ensure that the numerical results are independent of the grid size, a mesh independency study was carried out. Moreover, the turbulence is modeled by the $k - \omega$ SST turbulence model and the y^+ values at the solid walls are less than unity.

3.1. Flow Structure Characteristics

The proper analysis of the windage losses requires the detailed knowledge of the flow field. In this sense, the tangential velocity component defines the shear stress and its contribution to the torque required to rotate the rotor disk. Therefore, Figure 3 depicts the tangential velocity contour in the midplane of the rotor–stator configuration at $G = 0.0135$, $Re = 1.06 \times 10^5$, $\alpha_m = 0.8$ and $L = 0.0540$. This figure highlights the strong tangential velocity gradient between the magnet and the stator surface in the air-gap.

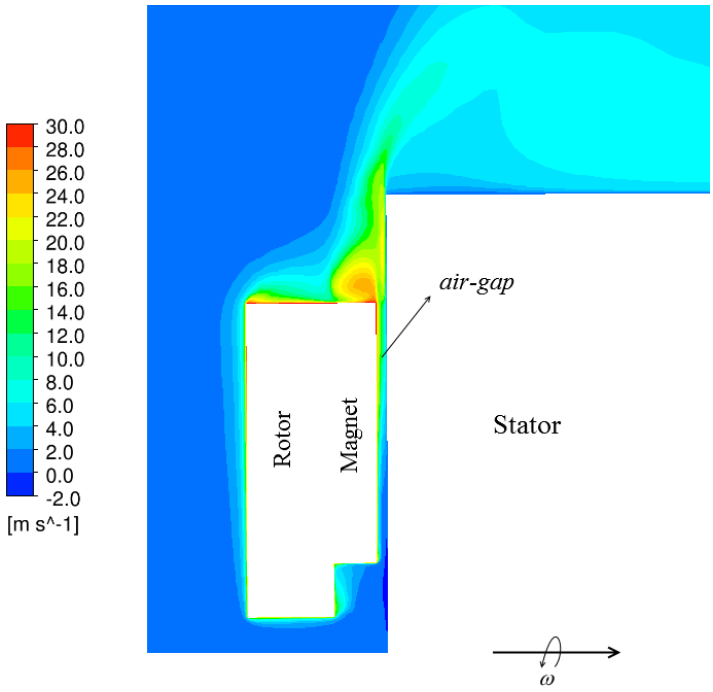

Figure 3. Absolute tangential velocity contour in the meridional plane through the center of the air-gap for $G = 0.0135$, $Re = 1.06 \times 10^5$, $\alpha_m = 0.8$ and $L = 0.0540$.

In addition, the contour of the relative tangential velocity at different radii in the air-channel is illustrated in Figure 4. It is seen that there is a significant gradient of the tangential velocity across the air-channel which elucidates the contribution of this region in the windage power losses of the machine. Furthermore, the positive and negative velocities in the air-channel demonstrate the presence of a vortex with radial core in this region.

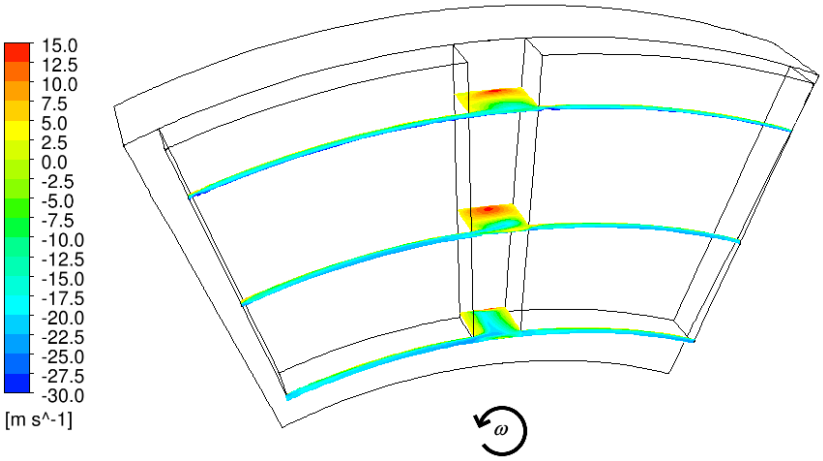

Figure 4. Relative tangential velocity contour across the air-channel for different radii at $G = 0.0135$, $Re = 1.06 \times 10^5$, $\alpha_m = 0.8$, and $L = 0.0540$. Positive values indicate a relative flow in the direction of the rotation.

To give more insight about the shear stress for the current discoidal system, the non-dimensional tangential velocity variations across the air-gap from the middle of the magnet to the stator surface (green lines in Figure 1a) at different radii have been shown in Figure 5. The left side of the axis belongs to the surface "*magnet front*" and the right side represents the stator surface in the gap. Two different flow patterns are observed according to the gap size distance. For the small gap size ratio $(G = 0.0068)$, the gradient of the tangential velocity at the higher radii is rather constant, typical for Couette flow. For the wide gap size $(G = 0.0811)$, however, the Stewartson type of flow is seen; that is to say, the tangential component of the velocity is almost zero everywhere except for the rotor boundary layer.

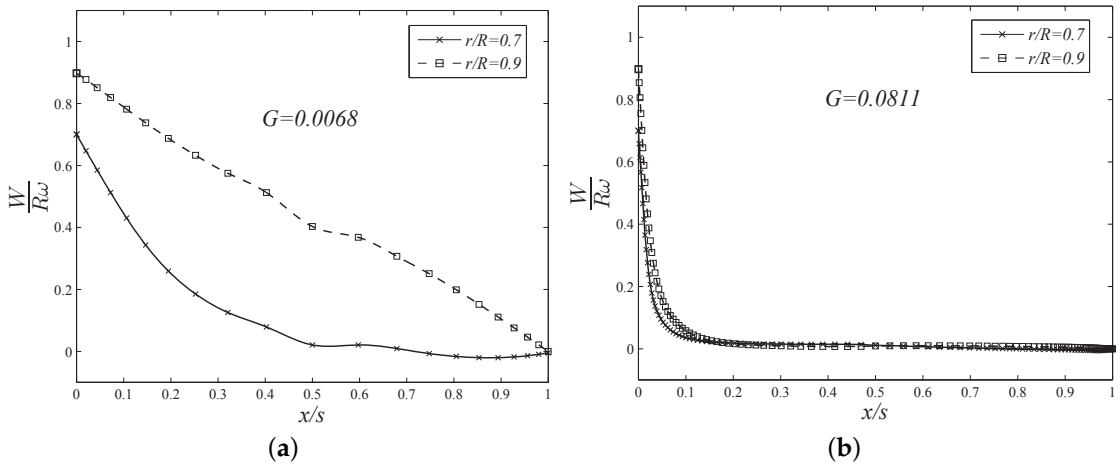

Figure 5. Non-dimensional tangential velocity $(\frac{W}{R\omega})$ across the air-gap at $Re = 1.06 \times 10^5$, $\alpha_m = 0.8$ and $L = 0.0540$ for (**a**) $G = 0.0068$ and (**b**) $G = 0.0811$. The left side of the axis belongs to the surface "*magnet front*" and the right side represents the stator surface in the gap.

On the other hand, the variations of the non-dimensional tangential velocity alongside of the air-channel (the red lines marked in Figure 1a) are depicted in Figure 6. Note that the left side of the horizontal axis denotes the point on the surface "*rotor facing stator*" in the middle between two magnets. It is noted that away from the rotor surface towards the stator surface in the air-channel, there is initially an increase in the tangential velocity magnitude, due to the presence of the vortex

within the channel, generated by the friction with the stator wall. The implication of this trend is that the surface "*rotor facing stator*" does not counteract the rotation of the disk.

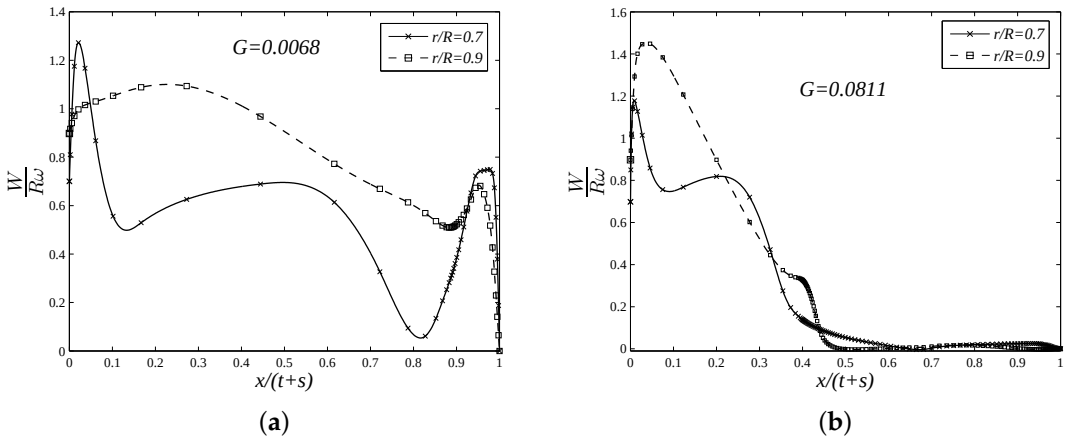

Figure 6. Non-dimensional tangential velocity ($\frac{W}{R\omega}$) across the air-channel at $Re = 1.06 \times 10^5$, $\alpha_m = 0.8$ and $L = 0.0540$ for (**a**) $G = 0.0068$; and (**b**) $G = 0.0811$.

In addition to the shear stress contribution in the windage losses, torque is also generated due to pressure forces, and depending on the actual geometry, this could give the largest contribution. The static pressure contour on the rotor disk with the magnets on it has been illustrated in Figure 7. Note that the other magnet has become visible through post-processing. As seen, there is a noticeable pressure difference between the surface of *"magnet left"* and *"magnet right"*, which, in turn, generates pressure forces acting against the rotary motion of the rotor disk. In this way, the side surfaces in the air-channel play an important role in the overall windage losses in the AFMPSM.

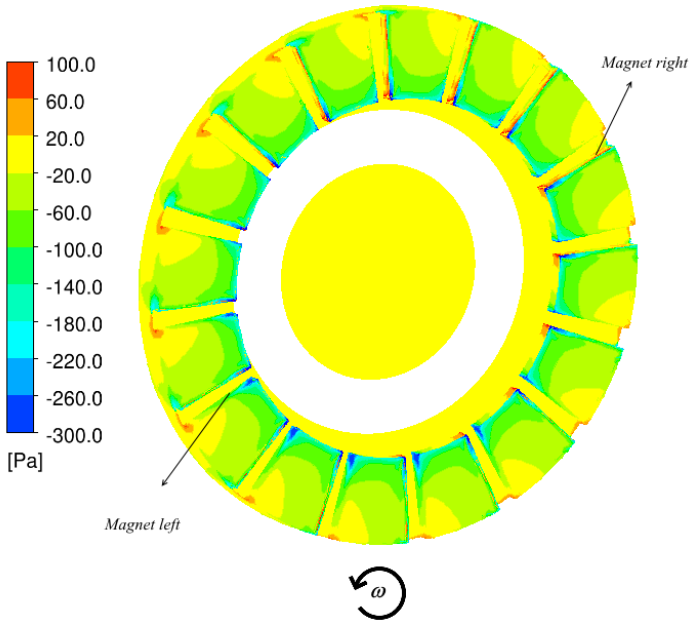

Figure 7. Static pressure contour on the rotor disk and the magnet at $G = 0.0135$, $Re = 1.06 \times 10^5$, $\alpha_m = 0.8$ and $L = 0.0540$.

3.2. Total Windage Power Losses

Figure 8 clarifies the influence of the gap size distance (s), the tip velocity of the magnet (V), the magnet angle (α) and the magnet thickness (t) on the overall windage power losses in the current arrangement.

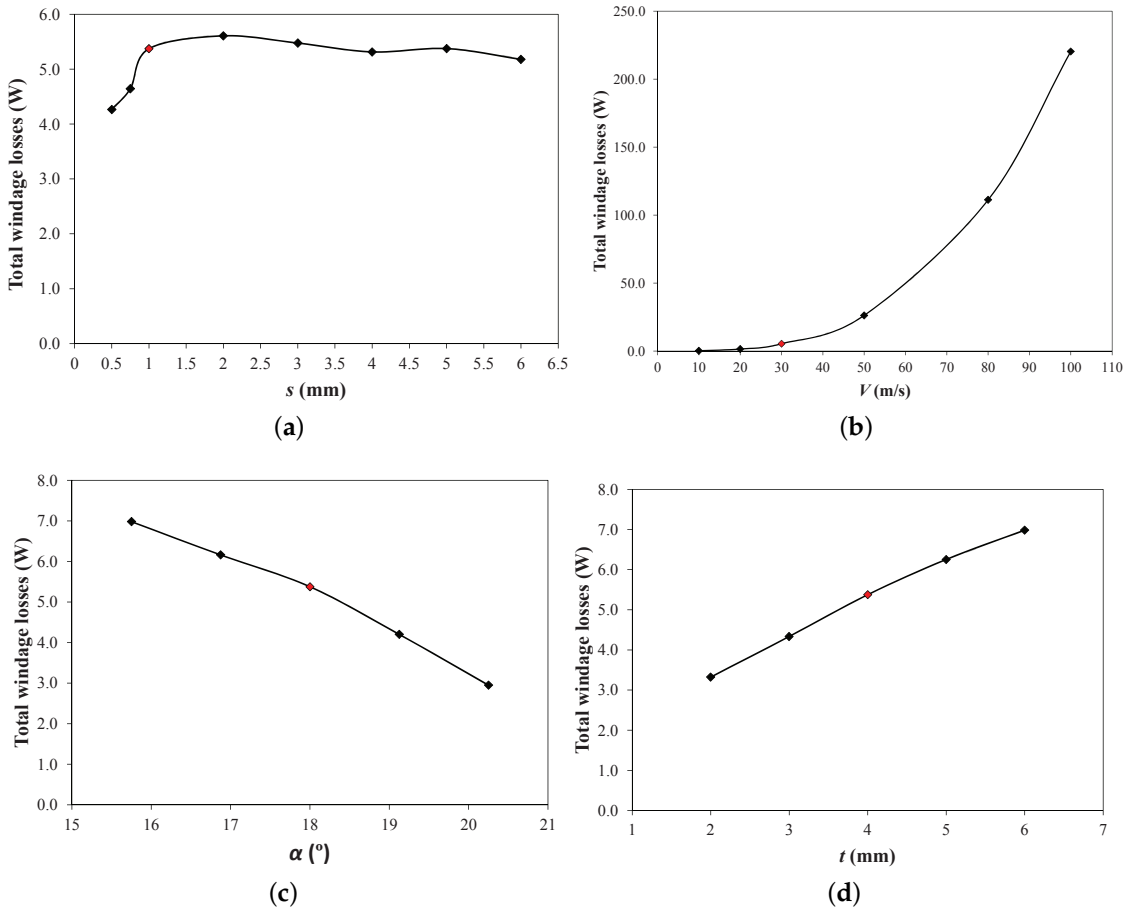

Figure 8. The influence of (**a**) gap size distance s (mm); (**b**) tip velocity of the magnets V (m/s); (**c**) magnet angle $\alpha(^\circ)$; and (**d**) magnet thickness t (mm) on the overall windage power losses (W) (reference point is highlighted with the red point).

Notice that by default the values of these geometrical parameters here are $s = 1$ mm, $V = 30$ m/s, $\alpha = 18^\circ$ and $t = 4$ mm, which are highlighted with the red dots in the figures. This reference point is equivalent to $G = 0.0135$, $Re = 1.06 \times 10^5$, $\alpha_m = 0.8$ and $L = 0.0540$. The overall losses have been computed by accumulating the losses generated at each individual surface. Note that the results of Figure 8 account for one rotor disk. The parametric study reveals that the rise of the rotational Reynolds number from 3.5×10^4 to 3.5×10^5 enormously increases the total windage losses from 0.2 to 220 W. Additionally, the iron losses in terms of excess, hysteresis, and dynamic losses substantially increase with an increase in the rotational speed [23]. This also gives rise to more copper losses as the skin effect in windings increases with frequency. Furthermore, the permanent magnet losses increase for greater values of the rotational speed.

The same trend, but very less profound, can be seen with variations of the magnet thickness ratio. In other words, the total windage losses climb by more than double as the magnet thickness ratio L varies from 0.0270 to 0.0811. The reason behind this behaviour is that the increase of the magnet thickness rises the contact area between airflow and the magnet, and not only that the area triples, but that this area, although relatively small, has a big impact on the losses because pressure is working there. However, from the electromagnetic point of view, the thicker permanent magnet (PM) leads to greater air-gap flux density resulting in a more efficient machine. At a certain point, additional increase in the PM thickness will bring about additional cost without any added value to the electromagnetic performance.

By contrast, as the magnet angle α enlarges from 15.75° to 20.25°, the overall windage power losses diminished by about 60%. The implication is that a wider magnet angle shrinks the total size of the air-channel, resulting in a decrease in the air mass flow rate inside the air-channel between the consecutive magnets, which lowers the windage losses. In view of the electromagnetic analysis, wider PM magnet angle results in more air-gap flux density as well as more a efficient machine. This, however, increases the volume of the PM, which, in turn, raises the PM losses.

On the other hand, the gap size ratio exhibits a discernible trend, that is, there is a growth in the overall windage losses, in the course of the transition from the very narrow gap to the wide gap size. As the gap size distance becomes larger, the value of the windage losses remains almost unchanged. It can be deduced that the gap size distance greater than nearly 2 mm does not affect the amount of the air mass flow rate entering into the air-channel, and the overall windage losses accordingly. It is interesting to say that the same behaviour was reported by Luo et al. [18]. Unlike the windage losses variations, an increase in the air-gap distance, while keeping the same PM width, deteriorates the electromagnetic performance of the machine.

4. Correlations for Windage Losses

The purpose of the CFD simulations is not only to perform the parametric study, but more importantly, to construct the correlations for the overall windage power losses in the AFPMSM under investigation. As shown before in Figure 1b, there are eleven surfaces in this system, namely hole lower, hole upper, rotor facing stator, rotor left side, magnet front, magnet lower, magnet left, magnet right, magnet upper, rotor sidewall and shaft, contributing to the overall windage losses in the machine. The idea is to find the formulations for the windage losses of each surface with respect to the gap size ratio, the rotational Reynolds number, the magnet angle ratio and the magnet thickness ratio. To make the correlations applicable for different scales of the AFPMSMs, it is required to express the windage losses as non-dimensional numbers. Since the windage losses occur as a result of two different sources; i.e, the viscous forces and the pressure forces, two distinct non-dimensional numbers should be defined. The windage power losses can be expressed as the following function:

$$P = f(\mu, \rho, \omega, R). \tag{1}$$

Note that R is the outer radius of the rotor which is also the length scale of the machine. According to the non-dimensional analysis, the non-dimensional windage power losses, $P^{'}$, can be written as

$$P^{'} = P\mu^{a}\rho^{b}\omega^{c}R^{d}. \tag{2}$$

The windage losses due to viscous forces scale proportional to the viscosity. Therefore, a is chosen to be -1. From this should then follow that $b = 0$. The other unknown coefficients can be easily given through the non-dimensional analysis. Thus, the non-dimensional windage losses due to the viscous forces on the surface, f, can be expressed as

$$P^{'}_{f,v} = \frac{P_f}{\mu\omega^2 R^3}. \tag{3}$$

On the other hand, the non-dimensional windage losses due to pressure forces scale proportional to the density. Thus, b is chosen to be -1. From this should then follow that $a = 0$. In the same manner, the unknown coefficients can be obtained by considering non-dimensional analysis. After that, the non-dimensional windage losses due to the pressure forces on the surface, f, are given by the following formulation:

$$P'_{f,p} = \frac{P_f}{\rho\omega^3 R^5}. \tag{4}$$

In above formulations, $P'_{f,v}$ and $P'_{f,p}$ are the non-dimensional windage losses for surface f due to viscous forces and pressure forces, respectively; P_f denotes the windage losses generated in surface f, μ is dynamic viscosity of air and ρ represents air density.

It is obvious that only two surfaces, namely "*magnet left*" and "*magnet right*" give rise to the windage losses due to the pressure forces, and the rest of the surfaces contribute to the windage losses because of the viscous forces. As a matter of fact, for both surfaces "*magnet left*" and "*magnet right*", the contribution of the viscous forces is even negligible, which explains the different choices of variables to make the contribution to the power dimensionless for these surfaces. To construct the correlations, a set of CFD simulations are performed for $G = \{0.0068, 0.0101, 0.0270, 0.0405, 0.0541, 0.0676, 0.0811\}$, while the other parameters are kept at the reference point, i.e., $\{Re = 1.06 \times 10^5, \alpha_m = 0.8, L = 0.0540\}$. Afterwards, $P'_{f,v}$ and $P'_{f,p}$ are computed according to Equations (3) and (4). By doing so, the variations of the windage power losses with G when other parameters are fixed at the reference point are given. The same procedure, as explained for G, is repeated when Re, α_m and L are being changed. In this way, the variations of $P'_{f,v}$ and $P'_{f,p}$ for each corresponding surface within the machine at different non-dimensional parameters will be known. In the end, it is necessary to provide formulations to express the non-dimensional windage losses as follows:

$$\begin{aligned} P'_{f,v} &= Z_f\left(G, Re, \alpha_m, L\right), \\ P'_{f,p} &= X_f\left(G, Re, \alpha_m, L\right), \end{aligned} \tag{5}$$

where the functions Z_f and X_f need to be defined. It is assumed that these functions with four variables can be rewritten as the product of four functions with one variable as

$$\begin{aligned} P'_{f,v} &= P'^{*}_{f,v} z_{f,1}(G) \times z_{f,2}(Re) \times z_{f,3}(\alpha_m) \times z_{f,4}(L), \\ P'_{f,p} &= P'^{*}_{f,\rho} x_{f,1}(G) \times x_{f,2}(Re) \times x_{f,3}(\alpha_m) \times x_{f,4}(L), \end{aligned} \tag{6}$$

where the superscript * represents the values of $P'_{f,v}$ and $P'_{f,p}$ at the reference point. To find all of the above functions with one variable, curve fitting for each case should be carried out one after the other. Evidently, the output from each function at the reference point is almost one. As discussed, there are two categories of surfaces in the current system: those where the windage losses are a result of the viscous forces and those where the windage losses are due to the pressure forces. The details of the formulations with respect to this classification of the surfaces are demonstrated in Tables 1 and 2.

Table 1. Correlations to estimate the windage losses (W) due to viscous forces.

Surface	Hole Lower, $f = 1$	Hole Upper, $f = 2$	Rotor Facing Stator, $f = 3$	Rotor Left Side, $f = 4$	Magnet Front, $f = 5$	Magnet Lower, $f = 6$	Magnet Upper, $f = 9$	Rotor Sidewall, $f = 10$	Shaft, $f = 11$
$P'^{*}_{f,v}$	5.600	42.108	-20.796	420.403	251.028	62.156	27.902	150.382	2.868
$z_{f,1}$	$0.6065G + 1.004$	$1.505G + 0.9783$	$-4.389 \times 10^{-7}G^{-2.942} + 1.112$	1	$0.8593G + 0.9902$	$-1.9016G^{0.4745} + 1.231$	$0.6994G^{-0.09581}$	$1.894G + 0.9848$	$11.76G + 0.8452$
$z_{f,2}$	$6.144 \times 10^{-6}Re + 0.3495$	$5.225 \times 10^{-6}Re + 0.4248$	$-17.19Re^{-0.07896} + 7.895$	$6.423 \times 10^{-6}Re + 0.3119$	$6.324 \times 10^{-6}Re + 0.3254$	$0.0007882Re^{0.6173}$	$1.023 \times 10^{-5}Re - 0.08718$	$7.285 \times 10^{-6}Re + 0.2174$	$4.432 \times 10^{-6}Re + 0.5308$
$z_{f,3}$	$-0.6796\alpha_m + 1.57$	$-0.6358\alpha_m + 1.502$	$-8.61\alpha_m^{4.393} + 4.212$	$0.2052\alpha_m + 0.8358$	$3.551\alpha_m^{23.38} + 0.9882$	$3.551\alpha_m^{23.38} + 0.9882$	$1.854\alpha_m^{9.287} + 0.7816$	$-0.7086\alpha_m + 1.579$	$-0.144\alpha_m + 1.114$
$z_{f,4}$	$-0.7068L + 1.035$	$0.664L + 0.9677$	$-7311L^{3.265} + 1.518$	$0.4958L + 0.9742$	$2.715L + 0.8581$	$20.74L - 0.1176$	$13.88L + 0.2696$	$2.688L + 0.8593$	$9.633L + 0.4791$

Table 2. Correlations to estimate the windage losses (W) due to pressure forces.

Surface	Magnet Left, $f = 7$	Magnet Right, $f = 8$
$P'^{*}_{f,\rho}$	0.02218	0.00527
$x_{f,1}$	$0.688G^{-0.2192} - 0.7961$	$-0.01947G^{-1.104} + 3.299$
$x_{f,2}$	$0.1116Re^{0.1866}$	$-1.633 \times 10^{8}Re^{-1.806} + 1.121$
$x_{f,3}$	$-3.876\alpha_m + 4.101$	$-7.127\alpha_m^{10.56} + 1.645$
$x_{f,4}$	$142.4L^{1.703}$	$-1.708 \times 10^{4}L^{3.453} + 1.733$

4.1. Robustness of the Correlations

It is worth mentioning that the same CFD simulations used in this work have been successfully employed to construct the correlations for the convective heat transfer modeling in the AFPMSM [22]. More importantly, the results were verified with the numerical simulations by Wrobel et al. [21] as well as the experimental data by Howey et al. [24]. This verification can give us trust in the CFD modeling used in this study.

The correlations presented in this paper have been obtained by varying one non-dimensional parameters while keeping the other parameters at the reference point and repeating this for all the other variables. As a result, to ensure the robustness of the correlations, a comparison should be made with CFD simulations for the cases where neither G, Re, α_m nor L is at the reference point. Table 3 demonstrates these comparative studies for four different cases. It is seen that the percentage error, $Error\% = |\frac{P_{f,CFD} - P_{f,Correlation}}{P_{Overall,CFD}}| \times 100$, is less than 3%, which indicates the efficacy of the presented correlations. The numerator represents the difference between the estimated windage losses on the surface, f, through CFD simulation and those predicted by proposed correlations. Moreover, the denominator refers to the overall windage losses through CFD simulation, which can be given by summing up the losses in each surface within the machine. It is observed that the values of windage losses for the surface *"rotor facing stator"* are negative, corresponding to the case where the flow was helping the rotary motion of the rotor disk as explained above in Figure 6. Another interesting point from Table 3 is that the proportion of the windage losses due to pressure forces is dominant as a whole in the AFPMSM under investigation.

The results of the correlations for the variations of windage losses due to viscous forces for the surfaces in the gap are also compared with the results reported by Wrobel et al. [21] in Figure 9, and a good agreement is observed. It should be mentioned that the computational domain is slightly different than the case in this paper as the rotor with magnets along with the stator disk are enclosed in a box with the prescribed ambient temperature. After all, it can be realized that the correlations presented in this paper are able to assess accurately the windage power losses for all surfaces in the practical ranges of the important parameters in AFPMSMs.

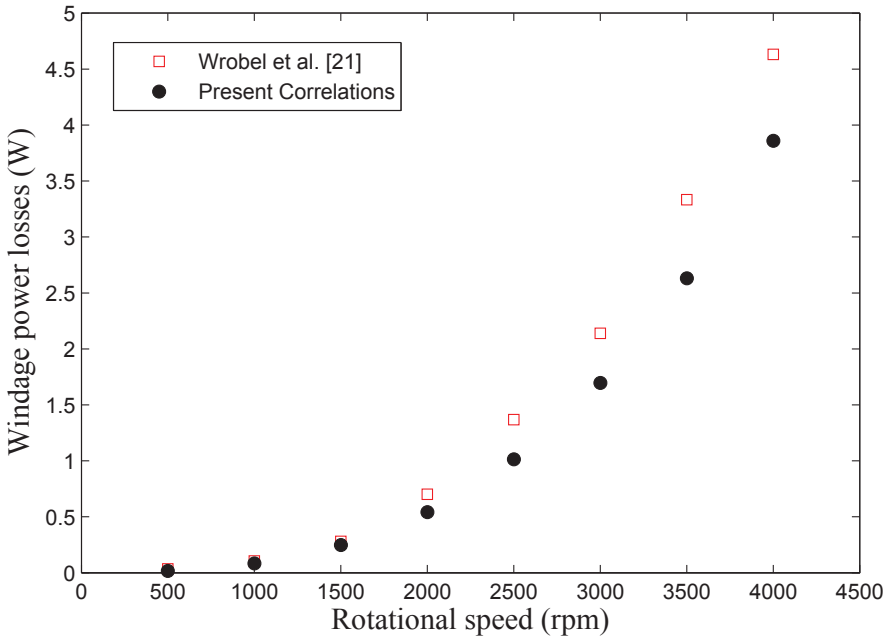

Figure 9. Comparison of the results of the windage losses due to viscous forces for surfaces in the gap region with the data reported by Wrobel et al. [21] at $G = 0.0156$, $L = 0.0376$ and $\alpha_m = 0.8$.

Table 3. Comparison between the CFD and the proposed correlations results for windage losses (W) at different cases when $R_r = 74$ mm.

Surface	$Re = 8.931 \times 10^4$, $G = 0.0203$, $L = 0.0338$, $\alpha_m = 0.77$			$Re = 2.322 \times 10^5$, $G = 0.0203$, $L = 0.0338$, $\alpha_m = 0.77$			$Re = 1.210 \times 10^5$, $G = 0.0108$, $L = 0.0642$, $\alpha_m = 0.82$			$Re = 1.901 \times 10^5$, $G = 0.0108$, $L = 0.0642$, $\alpha_m = 0.82$		
	Proposed Correlations	**CFD**	**Error%**	**Proposed Correlations**	**CFD**	**Error%**	**Proposed Correlations**	**CFD**	**Error%**	**Proposed Correlations**	**CFD**	**Error%**
hole lower	0.005	0.005	0.01	0.067	0.070	0.00	0.012	0.012	0.00	0.041	0.040	0.00
hole upper	0.039	0.037	0.07	0.478	0.457	0.00	0.087	0.083	0.00	0.277	0.276	0.00
Rotor facing stator	−0.055	−0.041	0.51	−0.747	−0.428	0.01	−0.005	−0.013	0.00	−0.022	−0.039	0.00
Rotor left side	0.365	0.355	0.34	5.096	4.888	0.00	0.891	0.878	0.00	3.113	3.052	0.00
Magnet front	0.204	0.206	0.07	2.809	2.811	0.00	0.562	0.548	0.00	1.940	1.897	0.00
Magnet lower	0.031	0.029	0.06	0.392	0.356	0.00	0.156	0.160	0.00	0.508	0.522	0.00
Magnet left	0.649	0.727	2.68	15.897	15.281	0.01	6.811	6.599	0.03	28.085	27.861	0.01
Magnet right	1.522	1.494	0.97	35.777	30.536	0.08	−0.719	0.170	0.11	−2.686	0.627	0.10
Magnet upper	0.020	0.016	0.14	0.316	0.297	0.00	0.062	0.082	0.00	0.214	0.327	0.00
Rotor sidewall	0.144	0.128	0.56	1.963	1.888	0.00	0.324	0.325	0.00	1.141	1.170	0.00
Shaft	0.002	0.002	0.00	0.024	0.026	0.00	0.006	0.006	0.00	0.019	0.020	0.00

4.2. Windage Losses at Magnet Surfaces

Since a great deal of the windage power losses occur on the magnet surfaces, the surfaces "*magnet front*" and a combination of "*magnet left*" and "*magnet right*" are precisely investigated in this section. It is worth highlighting that the surface "*magnet front*" contributes to the windage losses as a result of the viscous forces, whereas the other ones are responsible for the windage losses due to pressure forces.

Figures 10 and 11 illustrate the variations of $P_v^{'}$ and $P_p^{'}$ versus G for the surfaces "*magnet front*" and the sum of surfaces "*magnet left*" and "*magnet right*" at various non-dimensional parameters, respectively. It is perceived that $P_v^{'}$ slightly increases with G, which can be attributed to the transition from the narrow gap to the wide gap size (see Figure 5). Likewise, the variation of $P_v^{'}$, the same interpretation, in the case of the narrow gap, can be applied to the variation of $P_p^{'}$ for the side surfaces of the magnet, as more air is allowed to enter to the air-channel. For the wide gap size ratio, however, the flow path is shifted away more into the air-gap as compared to the air-channel region, which, in turn, slightly reduces the value of $P_p^{'}$ for the side surfaces of magnets, i.e., "*magnet left*" and "*magnet right*". In a similar manner, the influence of the magnet angle can be inferred. In fact, higher α_m implies that less air enters into the air-channel so that $P_p^{'}$ declines with increasing α_m while the opposite trend is observed for the variations of $P_v^{'}$. In addition, both values of $P_v^{'}$ and $P_P^{'}$ grow with L, as the increase in the magnet thickness brings about more air passing between rotor and stator. As expected, an increase of the rotational Reynolds number makes $P_v^{'}$ and $P_p^{'}$ larger, although the latter is less affected. Needless to say, the effect of the rotational Reynolds number is greatly noticeable for the windage losses due to viscous force; i.e, variations of $P_v^{'}$.

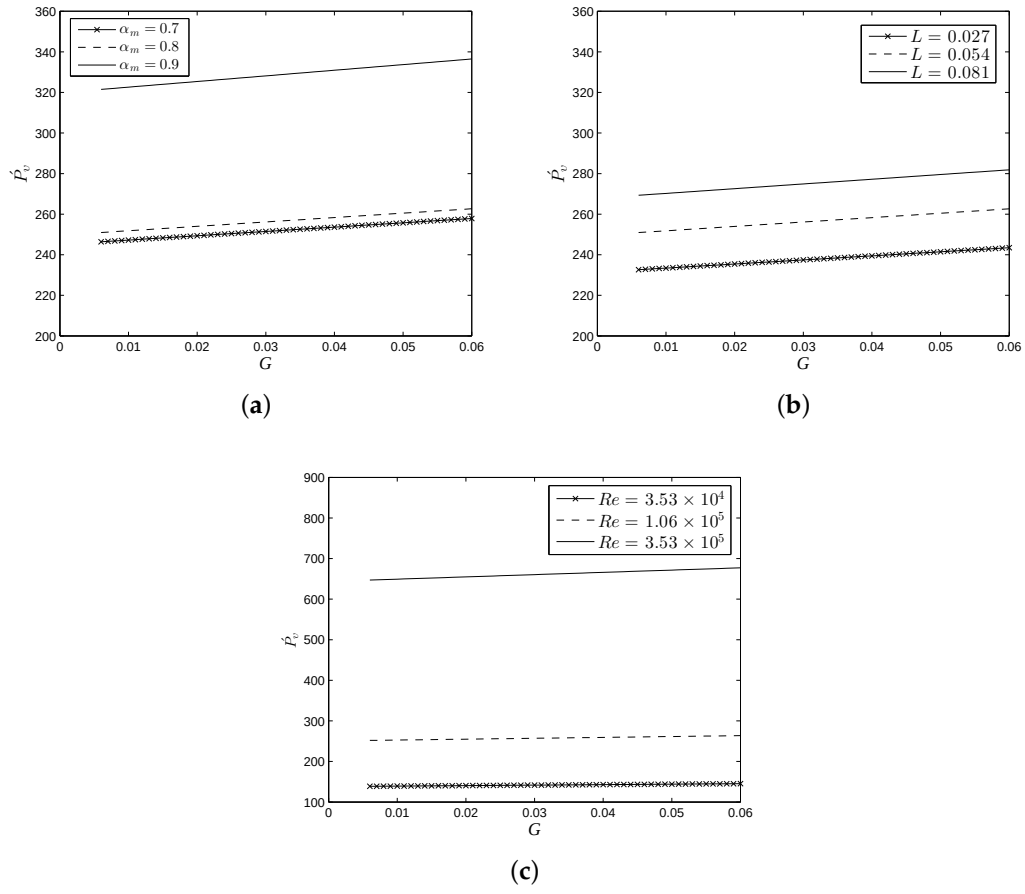

Figure 10. Variations of the dimensionless viscous power, $\acute{P}_v$, versus G for the *"magnet front"* surface at different values of (**a**) magnet angle ratio; (**b**) magnet thickness ratio; and (**c**) rotational Reynolds number.

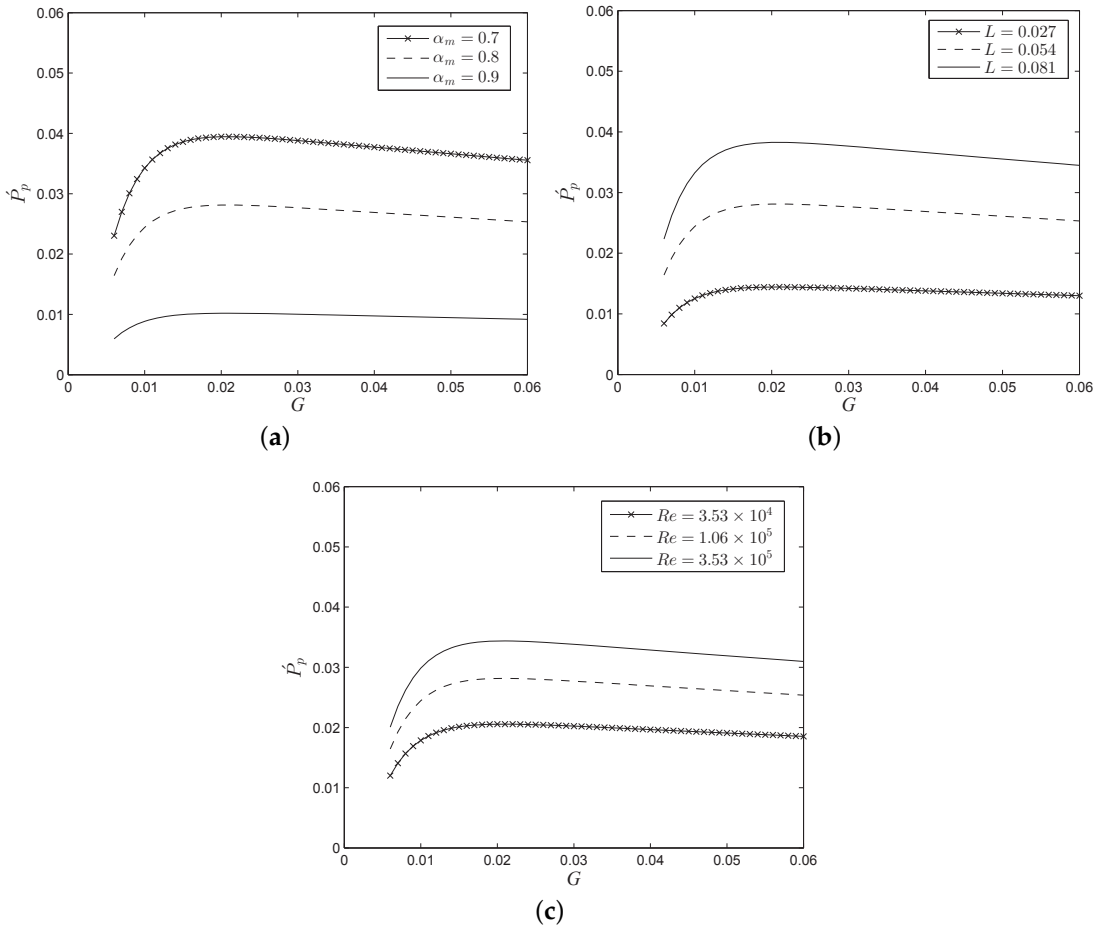

Figure 11. Variations of the dimensionless pressure power, $\acute{P}_p$, versus G for sum of side surfaces of the magnet ("*magnet left*" and "*magnet right*") at different values of (**a**) magnet angle ratio; (**b**) magnet thickness ratio; and (**c**) rotational Reynolds number.

5. Conclusions

The windage power losses in an axial flux permanent magnet synchronous machine have been studied in this research paper. Three-dimensional CFD simulations of the rotor–stator configuration with 16 magnets on the rotor disk were carried out with the aid of the Frozen Rotor method. The importance of the non-dimensional parameters such as the magnet thickness ratio, the magnet angle ratio along with the rotational Reynolds number and the gap size ratio on the flow fluid and their influences on the windage losses and the contributions from the different surfaces within the machine were analyzed. The variations of the tangential velocity component demonstrate that there exist two types of flow structures in the air-gap between the magnet and stator surface, that is, the Couette flow for the narrow gap and the Stewartson flow for the wide gap size ratio. Furthermore, the results of the parametric study indicate that the increase in the Reynolds number from 3.5×10^4 to 3.5×10^5 substantially increases the overall windage losses. In addition, the total windage losses become more than double as the magnet thickness ratio goes up from from 0.0270 to 0.0811. In contrast to variations of *Re* and *L*, the total windage losses drop by 60%, when the magnet angle ratio increases from 0.7 up to 0.9. The influence of the magnet geometrical parameters on the cooling improvement in the machine has been discussed by the authors [22], and these effects counterbalance the windage power losses' variations. As a result, the compromise should be made between the cooling system and the windage power losses in the design process of the machine.

In order to make the windage losses dimensionless, two formulations were introduced according to the cause of the losses whether they are due to the viscous forces or the pressure forces. After all, novel correlations for predicting the windage losses for the entire machine were constructed by means of curve fittings from the numerical data. It was concluded that the proposed correlations are quite robust and accurate in the practical ranges of AFPMSMs. The proposed correlations in this paper along with those recently presented for the convective heat transfer coefficients [22] can be employed in a coupled thermal, electromagnetical and mechanical losses analysis to fully optimize the performance of the machine.

Acknowledgments: The financial support for this study by Fonds Wetenschappelijk Onderzoek (FWO) project G.0110.13 is gratefully acknowledged.

Author Contributions: Each of the authors contributed to the preparation of this research paper. Alireza Rasekh performed the numerical simulations and wrote the paper. Jan Vierendeels provided critical comments in deriving the correlations. Peter Sergeant revised the manuscript substantially.

Conflicts of Interest: The authors declare no conflict of interest.

References

1. Vansompel, H.; Sergeant, P.; Dupr, L.; van den Bossche, A. Axial-flux PM machines with variable air gap. *IEEE Trans. Ind. Electron.* **2014**, *61*, 730–737.
2. Di Gerlando, A.; Foglia, G.M.; Iacchetti, M.F.; Perini, R. Parasitic currents in stray paths of some topologies of YASA AFPM machines: Trend with machine size. *IEEE Trans. Ind. Electron.* **2016**, *63*, 2746–2756.
3. Sergeant, P.; Vansompel, H.; Dupré, L. Influence of stator slot openings on losses and torque in axial flux permanent magnet machines. *Math. Comput. Simul.* **2016**, *130*, 22–31.
4. Huynh, C.; Zhneg, L.; Acharya, D. Losses in high speed permanent magnet machines used in microturbine applications. *J. Eng. Gas Turbines Power* **2009**, *131*, 1–6.
5. Mecrow, B.C.; Jack, A.G. Efficiency trends in electric machines and drives. *Energy Policy* **2008**, *36*, 4336–4341.
6. Luo, X.; Niu, S. Maximum Power Point Tracking Sensorless Control of an Axial-Flux Permanent Magnet VernierWind Power Generator. *Energies* **2016**, *9*, 581, doi:10.3390/en9080581.
7. Wang, Y.; Niu, S.; Fu, W. Electromagnetic Performance Analysis of Novel Flux-Regulatable Permanent Magnet Machines for Wide Constant-Power Speed Range Operation. *Energies* **2015**, *8*, 13971–13984.
8. Zhao, J.; Li, B.; Gu, Z. Research on an Axial Flux PMSM with Radially Sliding Permanent Magnets. *Energies* **2015**, *8*, 1663–1684.
9. Hua, W.; Zhou, L.K. Investigation of a Co-Axial Dual-Mechanical Ports Flux-Switching Permanent Magnet Machine for Hybrid Electric Vehicles. *Energies* **2015**, *8*, 14361–14379.
10. Huang, Y.; Guo, B; Hemeida, A; Sergeant, P. Analytical Modeling of Static Eccentricities in Axial Flux Permanent-Magnet Machines with Concentrated Windings. *Energies* **2016**, *9*, 892, doi:10.3390/en9110892.
11. Hemeida, A; Sergeant, P. Analytical Modeling of Surface PMSM Using a Combined Solution of Maxwell's Equations and Magnetic Equivalent Circuit. *IEEE Trans. Magn.* **2014**, *50*, 7027913.
12. Vranick, J.E. *Prediction of Windage Power Loss in Alternators*; NASA Technical Note; NASA Lewis Research Center: Cleveland, OH, USA, 1968; Volume 4849, pp. 1–18.
13. Wild, P.M.; Djilali, N.; Vickers, G.W. Experimental and computational assessment of windage losses in rotating machinery. *J. Fluids Eng.* **1996**, *118*, 116–122.
14. Anderson, K.R.; Lin, J.; McNamara, C.; Magri, V. CFD study of forced air cooling and windage losses in a high speed electric motor. *J. Electron. Cool. Therm. Control* **2015**, *5*, 27–44.
15. Sadeghierad, M.; Darabi, A.; Lesani, H.; Monsef, H. Rotor yoke thickness of coreless high-Speed Axial-Flux permanent magnet generator. *IEEE Trans. Magn.* **2009**, *36*, 2032–2037.
16. El-Hasan, T.S.; Luk, P.C.K.; Bhinder, F.S.; Ebaid, M.S. Modular design of high-speed permanent-magnet Axial-Flux generators. *IEEE Trans. Magn.* **2000**, *36*, 3558–3561.
17. Coren, D.; Childs, P.R.N.; Long, C.A. Windage sources in smooth-walled rotating disc systems. *J. Mech. Eng. Sci.* **2009**, *223*, 873–888.
18. Luo, X.; Zhang, D.; Tao, Z.; Xu, G.; Wang, Q. Windage measurements in a Rotor-Stator system with superimposed cooling and rotor-mounted protrusions. *J. Eng. Gas Turbines Power* **2014**, *136*, 1–11.

19. Liu, D.; Taho, Z.; Luo, X.; Kang, W.; Wu, H.; Yu, X. Investigation on the impact of protrusion parameter on the efficiency of converting additional windage loss for Ingress alleviation in rotor–stator system. *J. Eng. Gas Turbines Power* **2016**, *112604*, 1–9.
20. Giovanni, A. Numerical Investigations of Air Flow and Heat Transfer in Axial Flux Permanent Magnet Electrical Machines. Ph.D. Thesis, Durham University, Durham, UK, 2010.
21. Wrobel, R.; Vainel, G.; Copeland, C.; Duda, T.; Staton, D.; Mellor, P.H. Investigation of mechanical loss components and heat transfer in an Axial-Flux PM machine. *IEEE Trans. Ind. Appl.* **2015**, *51*, 3000–3011.
22. Rasekh, A.; Sergeant, P.; Vierendeels, J. Fully predictive heat transfer coefficient modeling of an axial flux permanent magnet synchronous machine with geometrical parameters of the magnets. *Appl. Therm. Eng.* **2017**, *110*, 1343–1357.
23. Bertotti, G. General Properties of Power Losses in Soft Ferromagnetic Materials. *IEEE Trans. Magn.* **1988**, *24*, 621–630.
24. Howey, D.A.; Holmes, A.S.; Pullen, K.R. Measurement and CFD Prediction of heat transfer in air-cooled disc-Type electrical machines. *IEEE Trans. Ind. Appl.* **2011**, *47*, 1716–1723.